



# Variations of ionospheric profile parameters during solar maximum and comparison with IRI-2007 over Chung-Li, Taiwan

Y. J. Chuo

Department of Information Technology, Ling Tung University, 408 Taichung, Taiwan

Correspondence to: Y. J. Chuo (yjchuo@teemail.ltu.edu.tw)

Received: 30 August 2011 – Revised: 15 July 2012 – Accepted: 7 August 2012 – Published: 23 August 2012

**Abstract.** This paper studies the seasonal changes in the diurnal variation of ionospheric bottomside slab thickness ( $B_0$ ), based on observations during high solar activities at the equatorial ionization anomaly (EIA) area station of Chung-Li (121.1° E, 24.9° N), Taiwan. The data examined in this investigation are derived from ionograms recorded at Chung-Li in 1999, and are compared with International Reference Ionosphere (IRI-2007) model values. In our data set  $B_0$  shows largest values and biggest changes during the daytime (06:00–12:00 LT) particularly in the summer. Moreover, the diurnal variation of  $B_0$  shows an abnormal peak during the pre-sunrise period, especially in the winter. The variation in the F-peak height ( $hmF_2$ ) is related to a thermospheric wind traveling toward the equator, which also enhances  $B_0$  during the pre-sunrise period. The results of the comparison with the IRI model show that  $B_0$  is overestimated, in both the  $B_0$ -table and the Gulyaeva option, after noon LT in the equinox ( $B_0$ -table and Gulyaeva average values for the overestimation are 11 and 47 km, respectively) and summer ( $B_0$ -table and Gulyaeva average values for the overestimation are 23 and 71 km, respectively) periods. Furthermore, the modeled values are underestimated at approximately 31 and 14 km for the table and Gulyaeva option during the daytime in the winter, respectively. The F2-layer maximum electron density ( $NmF_2$ ) data show reasonably favorable agreement with the model for a high correlation coefficient of approximately 0.97, with the major difference observed at approximately noon in the equinox and winter seasons. Regarding the  $hmF_2$  data, the model shows agreement with the observed values, and the largest discrepancy (average value is 39 km) was observed in the summer and the smallest (average value is 11 km) in the equinox season. This paper provides a comprehensive discussion on the relationship among  $B_0$ , the  $NmF_2$  and the  $hmF_2$  for geomagnetic storm events.

**Keywords.** Radio science (Ionospheric physics)

## 1 Introduction

Knowledge of the spatial distribution of the electron density in the ionosphere, especially the ionospheric profile  $N_e(h)$  is critical in applications, such as ionospheric empirical modeling, HF telecommunication, ionospheric tomography, GNSS operations (even if GNSS operations focus on total electron content (TEC), the electron density profiles must be known to understand TEC more clearly), and ionospheric studies. Such data are also useful in practical space weather applications and when modeling various physical processes in the ionosphere. The electron density profile for the ionospheric bottomside F2-layer is described regarding the F2-layer maximum electron density ( $NmF_2$ ), the thickness parameters,  $B_0$ , and the shape parameter,  $B_1$ , which represent the state of the bottomside region. In the International Reference Ionosphere (IRI) model, the electron density profile of the bottomside ionosphere is described using the following analytic expression (Ramakrishnan, and Rawer, 1972):

$$N_e(h) = NmF_2 \frac{\exp(-x^{B_1})}{\cosh(x)}, \quad x = \frac{hmF_2 - h}{B_0} \quad (1)$$

where  $hmF_2$  is the peak height of the F2-layer.

There are two options for calculating  $B_0$  in the IRI-2007 model. The first is the standard model, which uses a table of  $B_0$  values deduced from the profile inversion of ionograms at equatorial, low-, and mid-latitude stations (Bilitza, 2001). The other option (the so-called Gulyaeva option) is based on the Gulyaeva's model (Gulyaeva, 1987, 2007), which gives a relationship between the  $hmF_2$  and the half density height ( $h_{0.5}$ ) (Bilitza, 1990). The half density height is that below the F2 peak height where the electron density is half of the F2-peak density.

Several previous studies have investigated the variability of ionospheric bottomside profile parameters, such as those

**Table 1.** Monthly mean values of F10.7 solar flux and sunspot number in 1999.

Month	F10.7 solar flux	Sunspot number
1	138.1	62.0
2	138.6	66.3
3	124.9	68.8
4	118.8	63.7
5	151.0	106.4
6	175.2	137.7
7	171.0	113.5
8	175.0	93.7
9	137.2	71.5
10	163.7	116.7
11	187.4	133.3
12	164.5	84.6

by Ramanamurty and Rawer (1972), Reinisch and Huang (1996), Adeniyi and Radicella (1998), de Gonzales (1996), Bilitza et al. (2000), Sethi and Mahajan (2002), Abdu et al. (2004), Batista and Abdu (2004), Lazo et al. (2004), Lei et al. (2004), Zhang et al. (2004), Chen et al. (2006), Lee and Reinisch (2006), Lazo et al. (2007), Blanch et al. (2007), Adeniyi et al. (2008), McKinnell et al. (2009), Altadill et al. (2009), Sethi et al. (2009), and Oladipo et al. (2011). These studies have found that B0 shows appreciable diurnal, seasonal, and solar activity variations, which depend on the location of the observation station, whereas B1 exhibits little seasonal change. However, most previous studies have focused on the mid-latitudes and equator area. Few studies on the equatorial ionization anomaly (EIA) region have been conducted, and the northern crest of EIA in East Asia has not been studied. The complexity of the ionospheric formation increases in the EIA region. The EIA is characterized by a trough of the F2 layer peak electron density on the magnetic equator and by 2 humps at approximately 15° N/S of this point. The daytime development of the EIA occurs under the action of the E-region tide-induced dynamo electric field driving a vertical uplift of the F-region plasma, which then diffuses away from the magnetic equator under the pressure gradient force and gravity (Stening, 1992). The persistence of the EIA into the night hours depending on the season and solar activity, is known to be produced by the post-sunset enhancement in the eastward electric field generated by the F-region dynamo action. This dynamo action, in turn, results from the eastward component of the thermospheric wind blowing in the region of the decreasing dawn-to-dusk E-layer Pedersen conductivity distribution (Heelis, 2004).

The IRI model has been available for more than 30 years and has undergone a continual series of improvements since its first release in 1978 (Rawer et al., 1978; Bilitza, 1990, 1997, 2001; Bilitza and Reinisch, 2008). In the version IRI-2007, numerous changes have been made (Bilitza and Reinisch, 2008; Gulyaeva, 2007). In this paper, we analyze

the diurnal and seasonal variations of B0 and the *hmF2* using ionosonde observations over Chung-Li, Taiwan, during a period of high solar activity in 1999. Table 1 lists the monthly F10.7 solar flux and the sunspot number for the period of investigation. We then compare these observations with the IRI-2007 model to validate the IRI model over the northern crest of the EIA in East Asia. In addition, the effect of geomagnetic storms on B0, the *NmF2*, and the *hmF2* is presented and discussed. Such an investigation has not previously been undertaken in this area.

## 2 Data and analysis method

The Chung-Li ionosonde observation (24.9° N, 121.1° E), located in northern Taiwan and at the crest of EIA in East Asia, has significant advantages for studying EIA ionospheric dynamics. This paper lists a data set of more than 34 000 ionograms collected (routinely recording ionogram every 15 min) during high solar activity in 1999. Considerable effort was expended to scale these ionograms manually, so that the bottomside profiles could be calculated using the standard true-height inversion program POLAN (Titheridge, 1985). This allowed the critical frequency of the F2 layer (*foF2*), as well as the *hmF2* and B0, to be obtained. The data were grouped into 3 seasons for examination: equinox (March, April, September, and October), summer (May–August), and winter (November–February). The value of the *NmF2* is calculated according to the measurements of *foF2* from the ionograms:

$$NmF2 = 1.24(foF2)^2 \times 10^{10} \text{ el m}^{-3} \quad (2)$$

where *foF2* is in MHz.

The monthly averages (median values) of these parameters, which are the standard parameters in the ionosonde data set of the International Union of Radio Science (URSI), were then examined. Meanwhile, monthly medians were also used to compare the observational results with IRI-2007 model parameters for the same geophysical conditions and location. For the *NmF2* parameter, IRI-2007 offers 2 options: the first is recommended by CCIR (CCIR, 1966), and the second was developed by Rush et al. (1989) for URSI. In this study, the model-calculated values were obtained using both the table and Gulyaeva coefficients to compare them with the observations. We compare the IRI model result with the observations of B0, the *NmF2*, and the *hmF2*. Because IRI represents an average ionosphere, we use the monthly median values of *foF2*, the *hmF2*, and B0 for this comparative study.

## 3 Results

### 3.1 Experimental B0 and *hmF2*

Figure 1 shows the diurnal variations of B0 and the *hmF2*, compared to local time (LT) under high solar activity; the

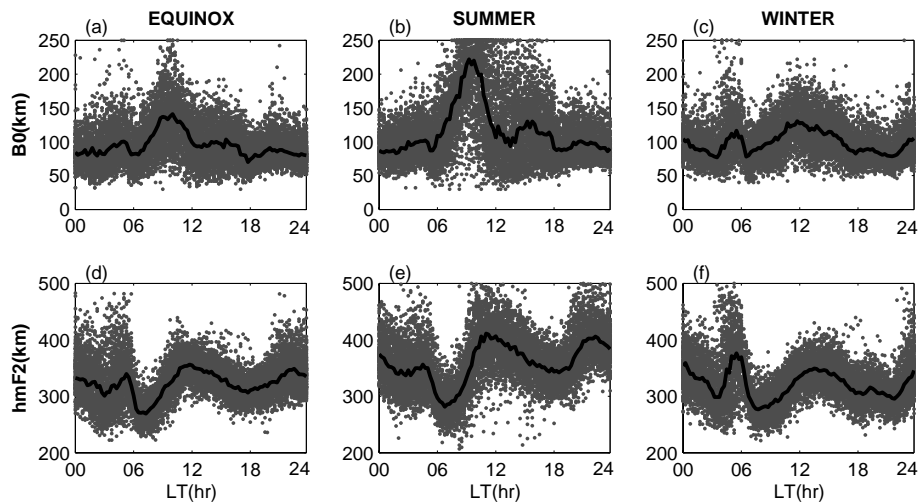


**Fig. 1.** Scatter plots (gray dots) and median values (solid line) show diurnal variation of  $B_0$  and  $hmF_2$  for (a), (d) equinox, (b), (e) summer, and (c), (f) winter, respectively.

corresponding median values are also provided. The results show a large day-to-day (dotted) and seasonal median (solid) variation for all seasons. The top panels (Fig. 1a–c) show the value of  $B_0$ , indicating that the lower values occur at night and the higher values occur during the day, especially in the summer. In the equinox, the median  $B_0$  (solid) increases from its nighttime value of approximately 80 km to a diurnal peak of approximately 145 km during the period 06:00–11:00 LT, then falls gradually until 17:30 LT before increasing again until 20:00 LT (Fig. 1a). In the summer,  $B_0$  begins to increase at 00:00 LT, and achieves its peak values of approximately 230 km at approximately 10:00 LT. This is followed by an abrupt decrease until 13:00 LT before increasing again to 130 km at 15:30 LT, and then falling back until 17:45 LT (Fig. 1b). Figure 1c shows the variation in  $B_0$  in the winter; the maximum value (approximately 130 km) occurs at 12:00 LT and a secondary higher peak (approximately 120 km) occurrence during the pre-sunrise period. This peak is stronger in the winter than in the equinox and summer. Figure 1d shows the diurnal variation plot for the  $hmF_2$  in the equinox. A higher peak is shown from 300–345 km during the period of 03:00–05:00 LT, and this rises from 06:00 LT to a maximum value of 355 km at 12:00 LT because of the daytime upward drift velocity (Fejer et al., 1991). For the summer, the observations showed that the  $hmF_2$  rises from 290 km to a maximum value of 410 km during the period 09:00–11:30 LT before falling gradually, and then increases again from 18:00 LT to 22:00 LT (Fig. 1e). In addition, a slight increase in the  $hmF_2$  occurs from 03:00 to 05:00 LT (340–355 km). In the winter, the maximum value (approximately 375 km) of the  $hmF_2$  occurs during the pre-sunrise period and suddenly decreases to 280 km at 07:30 LT, before gradually increasing again to 350 km during the period of

07:30–14:00 LT (Fig. 1f). The  $hmF_2$  then falls gradually, and rises to 330 km from 18:00 LT until 19:00 LT.

Figure 1 shows the seasonal variation of  $B_0$  and the  $hmF_2$ . This indicates that the daytime  $B_0$  values are higher in the summer and lower in the winter, and there is no apparent difference in nighttime  $B_0$  among the 3 seasons. Figure 1 shows that the  $hmF_2$  is higher during the daytime than nighttime in the summer and the very reverse in the winter. In addition, there are interesting phenomena with the 3 clear peaks in the  $hmF_2$  occurring at pre-sunrise, noon, and post-sunset in all 3 seasons. Meanwhile, there is a rapid decrease in  $B_0$  and the  $hmF_2$  during 05:00–06:00 LT. Furthermore, there are 2 clear increases during pre-sunrise and 06:00–11:00 LT period. For the pre-sunrise increase in  $B_0$ , it is observed in all 3 seasons, particularly in the winter. During the period of 03:00–05:00 LT, the  $hmF_2$  also shows an increase with the highest value in winter. The results indicate that the peak value in  $B_0$  is associated with the uplift of the F-layer during 03:00–05:00 LT in the winter. Krishnamurthy et al. (1990) studied the nighttime equatorial thermospheric winds and found that the neutral wind turns southward (equatorward) at 03:00 LT and resumes at 05:00 LT for low latitudes. The southward (equatorward) neutral wind induces an upward plasma drift. Consequently, the upward velocity does not only uplift the F-layer to a higher altitude, but also increases the  $B_0$  simultaneously. The daytime peak in  $B_0$  begins to increase at 06:00 LT and achieves a maximum value during 09:00–10:00 LT in the equinox and summer, and 12:00 LT in the winter. In the daytime period, the  $hmF_2$  increases beginning at 06:00 LT and achieves the maximum value during 11:00 LT in the equinox and summer, and 13:00 LT in the winter. However, the correlation between  $B_0$  and  $hmF_2$  variation during 06:00–13:00 LT is low in all 3 seasons (the correlation coefficient values are 0.152,  $-0.028$ ,

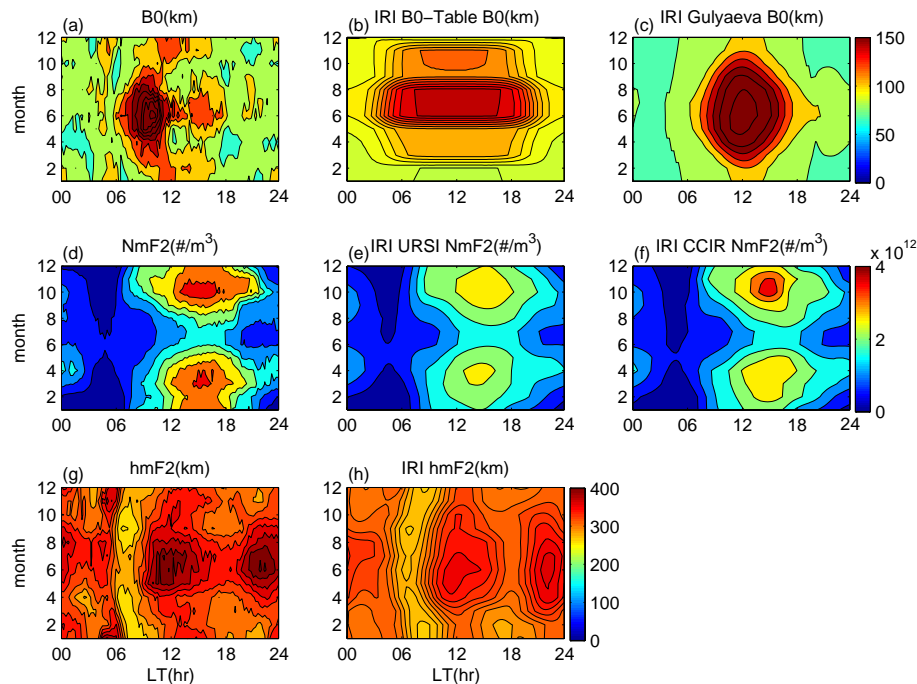


**Fig. 2.** Variations observed in the monthly median  $B_0$ ,  $NmF_2$ , and  $hmF_2$  values measured from ionosonde (left panels) and IRI-2007 (middle and right panels) during 1999.

and 0.508 for equinox, summer, and winter, respectively). After sunrise, the vertical plasma flow drift enhances and lifts the plasma to the higher altitudes on the equator, and the plasma then diffuses along the magnetic lines to low latitudes and increases the electron density. Fejer et al. (1995) studied the global plasma drift during the daytime on the equator and discovered that an upward plasma flow occurred during 06:00–09:00 LT in the equinox and summer, and lasted until 13:00 LT in the winter. The result shows a similar trend with  $B_0$  during 06:00–13:00 LT indicating that the vertical plasma flow drifts play an important role in  $B_0$  in the EIA region. Additionally, there is an apparent peak in the  $hmF_2$ , but not obvious for  $B_0$  during 18:00–22:00 LT. The gradually increasing  $hmF_2$  is associated with the equatorward thermospheric winds during 18:00–22:00 LT.

### 3.2 Comparison with IRI model

Figure 2 displays contour maps of the monthly median diurnal variations in  $B_0$ , the  $NmF_2$ , and the  $hmF_2$ . The left panels in this figure show the observed values, and the middle and right panels show values calculated using the IRI model for the period of high solar activity in 1999. Figure 2a indicates a seasonal variation for the observed value of  $B_0$ , and its diurnal value is lower at night and higher during the day. An apparent peak value occurred in the daytime during May–July. Figure 2b–c show the variations in  $B_0$  that were calculated using the B0-table and Gulyaeva options in the IRI model. Both modeled values also show the seasonal and di-

urnal variations. Both model options show some seasonal and diurnal variation in  $B_0$ . The daytime values in  $B_0$  are higher than nighttime and the summer values are higher than the other 2 seasons. However, the distribution of observed and modeled daily values is relatively different. For the  $NmF_2$  (Fig. 2, middle panels), a similar trend can be observed, with 2 apparent peak values occurring from 13:00 to 16:00 LT during March–May and October–November, and a trough from 04:00 to 06:00 LT in all seasons. Figure 2 also shows the variation of the  $hmF_2$  (bottom panels) for the observed (left) and IRI-modeled (middle) data. The same tendency can be seen, with 3 apparent peak values appearing at pre-sunrise, local noontime, and post-sunset, especially in the summer months. Figure 3 shows the diurnal variations of  $B_0$  (top panels), the  $NmF_2$  (middle panels), and the  $hmF_2$  (bottom panels) during the different seasons. The results show that the modeled values of  $B_0$  are overestimation of the observed (circled) values, for both the table (dotted) and Gulyaeva (solid) options in the period 12:00–19:00 LT in the equinox (the differences in average are approximately 11 km in the table option and 27 km in Gulyaeva) and summer (the differences in average are approximately 23 km in the table option and 71 km in Gulyaeva) seasons. The values of  $B_0$  show a seasonal and daily variation, with the highest values occurring at daytime in the summer and the lowest values in the nighttime in winter in both the table and Gulyaeva options. The modeled values that were obtained using the B0-table option show that  $B_0$  rises from 85 km at night to a maximum value (105 km) at 06:00 LT, before flattening and then decreasing at 18:00 LT.

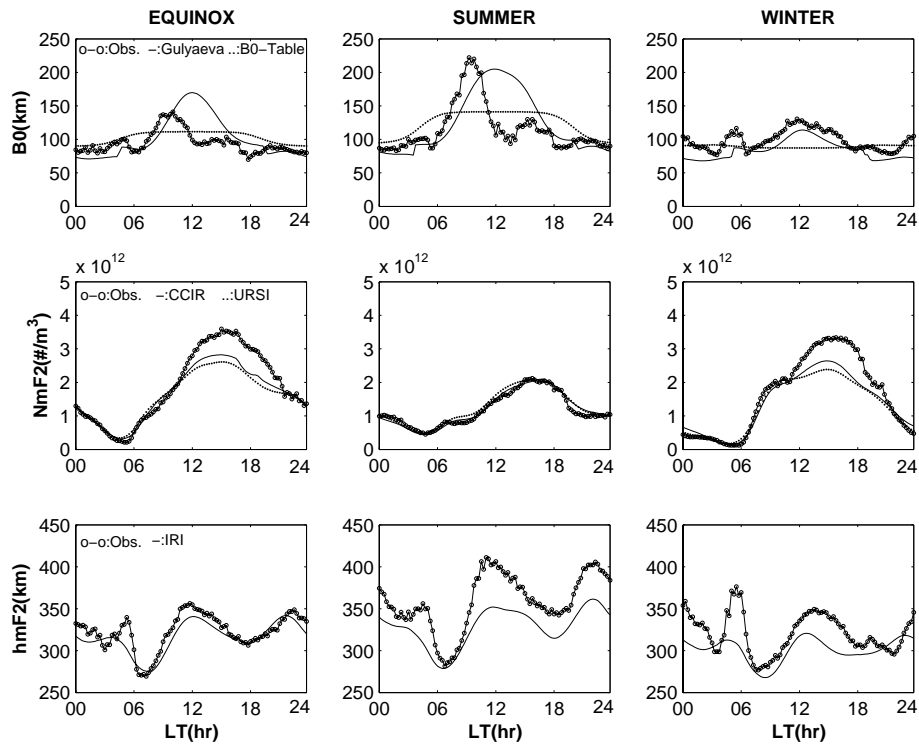


**Fig. 3.** Diurnal and seasonal variations in  $B_0$ ,  $NmF_2$ , and  $hmF_2$  measured from the ionosonde (circle) and IRI-2007 (solid and dotted) for the three seasons during 1999.

This flattened variation appears because the  $B_0$ -table option is simply a day–night transition function between a day value and a night value (Bilitza, 1990; Bilitza et al., 2000). The  $B_0$ -table values are overestimated (approximately 5–40 km) for much of the time, except from 08:00 to 11:30 LT in the equinox (approximately 30 km) and summer (approximately 70 km). In addition, the modeled values are underestimated for much of the winter, except for the pre-sunrise and post-sunset periods. Furthermore,  $B_0$ -table values are in favorable agreement with observations during 20:00–05:00 LT in the equinox and summer. The daily variation shows that  $B_0$  increases during the pre-sunrise and post-sunset periods, and the peaks are more obvious in the winter and summer. The 2 peaks cannot be obtained using the table-option; however, the peaks could be present in the Gulyaeva model. For the IRI-Gulyaeva (solid line), the modeled values are overestimated (10–100 km) during 11:30–19:30 LT and underestimated (3–10 km) during 19:45–11:30 LT in both the equinox and summer. In addition,  $B_0$  is consistently underestimated in the winter. Furthermore, small differences between the modeled and observed values are present during the period of 20:00–05:00 LT for all seasons, and the annual variation is closest to the observed values in the winter. The results show a favorable agreement between the Gulyaeva option and observations during 16:00–09:00 LT in the equinox and summer, and the entire day in the winter. The significant positive differences (approximately 117 %) between observations and the

Gulyaeva option occur during 10:00–15:00 LT in the summer and equinox. Moreover, the  $B_0$ -table option does not predict the pre-sunrise collapse and post-sunset increase behaviors according to the Chung-Li ionosonde. These results indicate that the Gulyaeva option reveals a similar trend of the observations, particularly in the winter. The middle panels of Fig. 3 show the variations in the  $NmF_2$  average values, and depict a comparison among CCIR (solid), URSI (dotted), and observed (circle) values over the same duration. The results show a seasonal and diurnal variation, with the maximum appearing during the daytime in the equinox and winter. The modeled and observed values are in favorable agreement regarding tendency for both CCIR and URSI modes, but for a larger underestimation during the local noontime, especially in the equinox and winter for high solar activities. In addition, the largest deviation in the comparison with the URSI and CCIR mode are  $1.14 \times 10^{12}$  and  $9.89 \times 10^{11}$  electron  $m^{-3}$ , occurring from 13:00 to 19:00 LT in both the equinox and winter. The bottom panels of Fig. 3 show the variation of the  $hmF_2$  in the observed (circle) and modeled (solid) data among the 3 seasons. The observed results show 3 apparent peaks at pre-sunrise, noon LT, and post-sunset in all 3 seasons. These phenomena could also be found in the modeled values, which show a similar tendency to the observed values, especially in the equinox season. Again, the modeled values in the  $hmF_2$  are underestimations of the observed values for much of the time in all seasons, especially in the

summer. The largest deviation between observed and modeled values occurs at 05:00–06:00 LT in the equinox (approximately 30 km) and winter (approximately 60 km), and during 10:00–11:00 LT in the summer (approximately 70 km).

### 3.3 Geomagnetic storms effect in B0, NmF2, and hmF2

This study also examined the response of the ionospheric bottomside profile parameter, B0, to 2 geomagnetic activity events. Figure 4 shows the variations of the Dst index, NmF2, the hmF2, and B0 for 2 geomagnetic storms during 5 consecutive days. The dotted and gray lines denote the observation and monthly medians, respectively. Figure 4a and e show the variation in the Dst index from 22 September to 26 September 1999 and 21 October to 25 October 1999, respectively. Two geomagnetic storms occurred on 23 September and 22 October 1999. In the first event, the sudden storm commencement (SSC) began at 05:00 LT (dashed line); a minimum value of the Dst index (−173 nT) was achieved at 08:00 LT, followed by a gradual recovery during 23 September to 26 September. Figure 4b shows the variation of the NmF2 during this period, and the lack of data since the strong seismic event (i.e. the Chi-Chi earthquake) led to the observation being shut down on 22 September. The NmF2 clearly increased after the SSC onset and then decreased on 23 September. From 24 September, a positive storm effect is apparent. Furthermore, the hmF2 shows an apparent variation and lift after 18:00 LT on 23 September, followed by a less pronounced downward trend on 24 September (Fig. 4c). A prominent increase in B0 occurred at the initial phase of the storm recovery on 23 September and a slight increase is apparent at approximately noon LT on 24 September (Fig. 4d). There were no significant changes during the other days. The effect on B0 is considered an increase during 13:00–18:00 LT on 23 September, and was accompanied by a decrease in NmF2 and no significant change in the hmF2. This decrease in the NmF2 could be caused by the changes of the atmospheric composition such that an increase in the N<sub>2</sub>/O ratio and also increases in the [H<sup>+</sup>]/[O<sup>+</sup>] ratio lead to the loss rate increasing. The [H<sup>+</sup>]/[O<sup>+</sup>] ratio plays an important role in the ionospheric shape forming. The increase in the N<sub>2</sub>/O ratio depends on the increase in the concentration of molecular N<sub>2</sub> or the decrease in atomic oxygen density. In addition, the increase in the N<sub>2</sub> concentration is believed to enhance the loss rate of [O<sup>+</sup>] (Prölss, 1995). The increase in NmF2 in the daytime on 24 September was associated with a slight decrease in the hmF2 and increase in B0. This suggests a vertical upward plasma flow to a higher altitude with a distribution of ionization at a greater height on the equator and then an expansion to lower latitudes, resulting in an increase in the electron density and also a poleward thermospheric wind to reduce the hmF2 at Chung-Li. The poleward thermospheric wind induces aligned motions in the plasma field and drags the plasma to a lower altitude, increases the loss rate, and moves the hmF2 downwelling (Maruyama et al.,

2007). Regarding the second event, Fig. 4e shows the variation of the Dst index during 21 October to 25 October 1999. An intense geomagnetic storm occurred on 22 October, with the SSC at 08:00 LT. The Dst index achieved its minimum values (−238 nT) at 16:00 LT, followed by a gradual recovery through the reset of the day on 22 October. Figure 4f–h shows the variation in the NmF2, the hmF2, and B0 during 21 October to 25 October 1999. The results show an increase and then a slight decrease in NmF2 after the storm onset on 22 October. In addition, the hmF2 exhibits a prominent uplift and an abrupt vibration on 22 October and at pre-sunrise on 23 October, and the B0 values increase simultaneously. The decrease in the NmF2 is associated with the increase in the hmF2 and B0 during the recovery phase during 22 October to 23 October. The increase in the hmF2 is attributed to the thermospheric winds traveling toward the equator, which are driven by auroral heating causing the atmospheric composition to change, leading to a decrease in the NmF2 and an increase B0 (Rishbeth et al., 1987; Davies and Liu, 1997). Because the decrease in the NmF2 occurs during 11:00–24:00 LT on 21 September, the Dst index shows a quiet condition in the geomagnetic field and the hmF2 and B0 show a slight increase approximately 20 and 15 km, respectively. However, Liu et al. (2004) studied the pre-earthquake ionospheric anomalies and mentioned that the decrease in the NmF2 could be associated with a strong earthquake occurrence on 22 October.

## 4 Discussion and conclusion

Ionosonde measurements taken at the Chung-Li observation station during 1999 were used to investigate the diurnal and seasonal variations of B0 and the hmF2. The observational data were also compared with the IRI-2007 model output to validate its predictions. For B0, the results indicate that a peak occurs from 03:00 to 05:00 LT, especially in the winter for high solar activities. Sethi and Mahajan (2002) studied the B parameters by using incoherent scatter measurements at Arecibo and observed the pre-sunrise peak in B0 during a solar maximum period. The hmF2 values also showed an increase during the same period, and their maximum also occurred in the winter. The nighttime winds are primarily toward equator in the pre-midnight sector, but for the midnight temperature maximum (MTM) occurs near the equator to turn the winds toward pole in the post-midnight, and soon after the meridian winds subsequent return to the equatorward direction in the pre-sunrise (Krishnamurthy et al., 1990; Batista et al., 1997). The increase in the hmF2 before sunrise is associated with the meridian neutral wind turning southward (equatorward) to produce the F-region uplift (Krishnamurthy et al., 1990). The post-sunset increase in B0 during different seasons at low latitudes can be attributed to the increasing of the NmF2 and the hmF2 (Lee et al., 2007). This increase in the NmF2 and hmF2 is associated with the

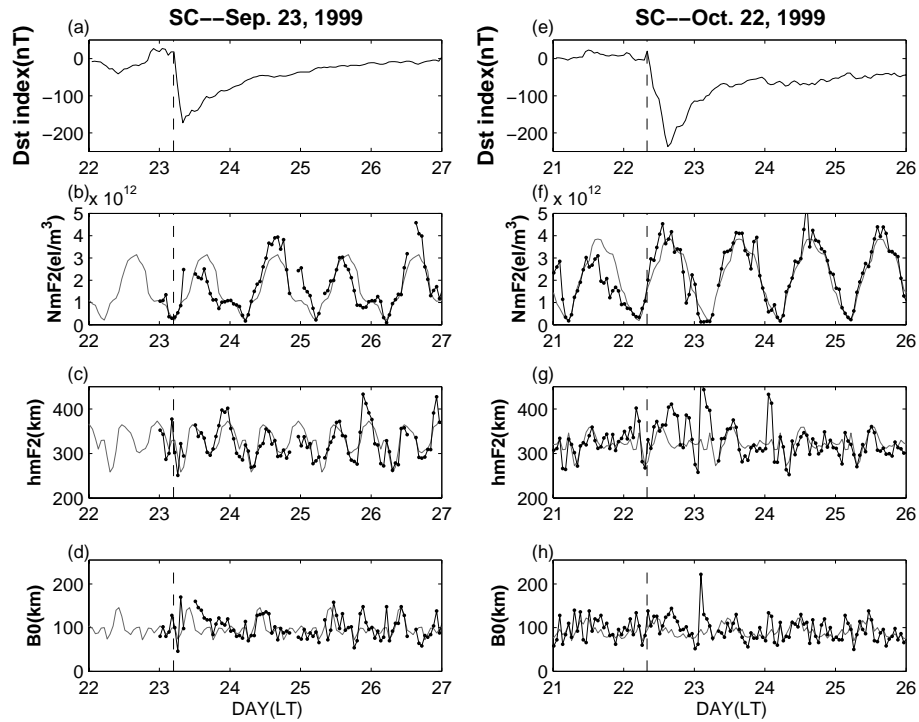


**Fig. 4.** Variations in Dst,  $NmF2$ ,  $hmF2$ , and  $B0$  parameters during a geomagnetic storm period on 23 September and 22 October 1999, respectively. The dotted and gray solid lines denote the observed and monthly median values, respectively. The vertical dash line denotes the SSC onset.

equatorial pre-reversal enhancement of the eastward electric field (Farley et al., 1986). In addition, the daytime collapse of  $B0$  during 09:00–12:00 LT occurs in the equinox and particularly in the summer. The combination of the variations in the  $hmF2$  and the  $NmF2$  can explain the occurrence of the daytime collapse of  $B0$ . The decrease in  $B0$ , combined with the increases in the  $NmF2$  and the  $hmF2$ , leads to the ionospheric shape flattening during this period. An increase in photoionization and the fountain effect from the equator produces an increasing number of electrons. The results were not observed on the equator during high solar activities (Sethi and Mahajan, 2002), even at low latitude in Hainan (Zhang et al., 2004). Furthermore, the collapse phenomena are not predicted by the IRI model. The smaller nighttime  $B0$  values are associated with the lower  $hmF2$ , smaller production rate, and greater loss rate on the equator (Lee and Reinisch, 2006). However, at the EIA, the  $hmF2$  shows an increase during the evening period, particularly in the summer. This uplift in the F-layer reduces the  $N_2/O$  ratio (Schunk and Nagy, 2000) and causes the slight peak of  $B0$  during the post-sunset. This phenomenon is predicted by Gulyaeva, but not the  $B0$ -table option in the IRI-2007 model. Regarding  $B0$ , daytime values are greater than those in the nighttime, and they are largest in the summer. The modeled values obtained using the Gulyaeva option generally agree more favorably with the observations than do those from the  $B0$ -table option. Moreover, we examined the study for using the true  $foF2$  and

**Table 2.** The rms deviation between modeled and observed values during three seasons.

	Equinox	Summer	Winter
$B0$ -IRI-Gulyaeva/ $B0$ -true	26.3407	39.0630	16.9983
$B0$ -IRI-Table/ $B0$ -true	16.0213	30.7181	18.3715

the  $hmF2$  as input parameters in the IRI model to predict the  $B0$  values and calculate the root mean square (rms) deviation based on the observed values. Table 2 shows the result of rms deviations between the modeled values and observation during the 3 seasons. It shows a minimum rms deviation in the equinox (16.0213) and winter (16.9983) for option  $B0$ -table and Gulyaeva, respectively.

For  $NmF2$ , the results show that the modeled values from both URSI and CCIR modes are generally close to the observed values. Significantly negative differences exist during 12:00–22:00 LT in the equinox and winter, and small negative deviations occur during the nighttime in the summer. These results differ from those obtained by Zhang et al. (2004), who conducted a comparative study for 6 months in 2002 by using the IRI-2001 model at a low-latitude station in Hainan and found that  $foF2$  values are in favorable agreement during the daytime and are underestimated for the nighttime. In addition, Batista and Abdu (2004) and Bertoni

et al. (2006) performed similar investigations of the south EIA crest and found that the IRI model overestimates the values of  $f_oF2$  at approximately 06:00 LT during April (autumn) and July (winter). Meanwhile, our results also show that the CCIR mode is slightly more effective when using the observed data than the URSI mode during the daytime in the equinox and winter.

For the  $hmF2$  parameter, the morphology of the diurnal variation is highly similar for all 3 seasons, with 3 peak values occurring at pre-sunrise, local noon, and in the evening hours. The most conspicuous peaks occur at pre-sunrise and local noon. Apparently, the pre-sunrise peak in B0 is caused by the equatorward atmospheric neutral wind to lift the F-layer toward higher altitudes. In addition, the pre-sunrise peak reduces the  $N_2/O$  ratio and causes an increase in B0. The noontime peak in B0 is attributed to the upward plasma flow on the equator, which is caused by the eastward electric fields. The  $[H^+]/[O^+]$  ratio is known to be crucial for the ionospheric shape (Davies and Liu, 1997). Therefore, after sunrise, the meridional neutral wind is oriented toward the pole and produces a diffusion effect from the topside ionosphere to lower altitudes. Furthermore, the effect of photoionization during the daytime still increases the bottomside ionospheric electron density. The evening peak is most pronounced in the summer season and is related to the equatorward thermospheric winds during the post-sunset period. The equatorward neutral wind lifts the F layer to higher altitudes and reduces the loss rate in  $[O^+]$ . After sunset, the photochemical ionization rapidly decreases and causes a decrease in the  $NmF2$ . By comparing the observation with the  $hmF2$  values provided by the IRI-2007 model, there are similar tendencies such as the 3 peaks occurring at pre-sunrise, local noon, and post-sunset. However, the modeled results are in poor agreement with the observations, and are usually underestimations of the observed value. The pre-sunrise peak is present, but unclear, and is greatly underestimated by the model, especially in the summer. However, the  $hmF2$  is in favorable agreement between the IRI and observations in the equinox.

Regarding the effect of the geomagnetic storms, the results indicate an increase in B0 during the initial periods at the EIA. The case studies showed an apparent increase in B0 during the first day after SSC onset. Although numerous highly complex mechanisms are at work, one mechanism is clearly responsible for the well-known daytime fountain effect, reducing the drift of ionization away from the equator, such as that observed during the September 1999 storm event; the other mechanism is attributed to the thermospheric winds traveling toward the equator, causing the atmospheric composition to change and the  $N_2/O$  ratio to decrease. This decreases the  $NmF2$  and increases the  $hmF2$ , as observed during the October 1999 storm event.

This investigation is the first to compare the ionospheric bottomside profile parameter, B0, and the F-layer peak height,  $hmF2$ , with the IRI-2007 model output over the Tai-

wan area. This is also the first comprehensive discussion of the effect of geomagnetic storms in the northern crest of the equatorial anomaly in East Asia. These results show that some improvements are still necessary to obtain realistic simulations results of the ionospheric EIA region.

*Acknowledgements.* The author greatly thanks Editor, reviewers and T. L. Gulyaeva for their valuable comments and suggestions. The author also thanks C. C. Lee for his discussion. We would like to thank the World Data Center (WDC) for providing data on the Dst index and the geomagnetic storm table. This work was supported by the grants of National Science Council NSC 100-2111-M-275-001 and NSC 101-2111-M-275-001.

Topical Editor K. Kauristie thanks three anonymous referees for their help in evaluating this paper.

## References

- Abdu, M. A., Batista, I. S., Reinisch, B. W., and Carrasco, A. J.: Equatorial F-layer heights, evening prereversal electric field, and night E-layer density in the American sector: IRI validation with observation, *Adv. Space Res.*, 34, 1953–1965, 2004.
- Adeniyi, J. O. and Radicella, S. M.: Variation of bottomside profile parameters B0 and B1 at high solar activity for an equatorial station, *J. Atmos. Solar Terr. Phys.*, 60, 1123–1127, 1998.
- Adeniyi, J., Radicella, S., Adimula, I., Willoughby, A., Oladipo, O., and Olawepo, O.: Validation of B0 and B1 in the IRI 2001 model at low solar activity for Ilorin an equatorial station, *Adv. Space Res.*, 42, 691–694, 2008.
- Altadill, D., Torta, J., and Blanch, E.: Proposal of new models of the bottom-side B0 and B1 parameters for IRI, *Adv. Space Res.*, 43, 1825–1834, 2009.
- Batista, I. S. and Abdu, M. A.: Ionospheric variability at Brazilian low and equatorial latitudes: comparison between observations and IRI model, *Adv. Space Res.*, 34, 1894–1900, 2004.
- Batista, I. S., Sastri, J. H., de Medeiros, R. T., and Abdu, M. A.: Nighttime thermospheric meridional winds at Cachoeira Paulista (23° S, 45° W): Evidence for effects of the equatorial midnight pressure bulge, *J. Geophys. Res.*, 2, 20059–20062, 1997.
- Bertoni, F., Sahai, Y., Lima, W. L. C., Fagundes, P. R., Pillat, V. G., Becker-Guedes, F., and Abalde, J. R.: IRI-2001 model predictions compared with ionospheric data observed at Brazilian low latitude stations, *Ann. Geophys.*, 24, 2191–2200, doi:10.5194/angeo-24-2191-2006, 2006.
- Bilitza, D.: International Reference Ionosphere 1990, NSSDC/WDC-AR&S 90-22, Natl. Space Sci. Data Cent., Greenbelt, Md., 1990.
- Bilitza, D.: International Reference Ionosphere – status 1995/96, *Adv. Space Res.*, 20, 1751–1754, 1997.
- Bilitza, D.: International reference ionosphere 2000, *Radio Sci.*, 36, 261–275, 2001.
- Bilitza, D. and Reinisch, B. W.: International Reference Ionosphere 2007: improvements and new parameters, *Adv. Space Res.*, 42, 599–609, 2008.
- Bilitza, D., Radicella, S. M., Reisch, B., Adeniyi, J., Mosert, M., Zhang, S., and Obrou, O.: New B0 and B1 models for IRI, *Adv. Space Res.*, 25, 89–96, 2000.

- Blanch, E., Arrazola, D., Altadill, D., Buresova, D., and Mosert, M.: Improvement of IRI B0, B1 and D1 at mid-latitude using MARP, *Adv. Space Res.*, 39, 701–710, 2007.
- CCIR: Comité Consultatif International des Radiocommunications, Report 340-1 and 340-6, International Telecommunication Union, Geneva, Switzerland, 1966.
- Chen, H., Liu, L., Wan, W., Ning, B., and Lei, J.: A comparative study of the bottomside profile parameters over Wuhan with IRI-2001 for 1999–2004, *Earth Planets Space*, 58, 601–605, 2006.
- Davies, K. and Liu, X. M.: Ionospheric slab thickness in middle and low-latitudes, *Radio Sci.*, 26, 997–1005, 1997.
- de Gonzalez, M. M.: Observed and model  $N(h)$  profiles for two Argentine stations, *Adv. Space Res.*, 18, 53–56, 1996.
- Farley, D. T., Bonelli, E., and Fejer, B. G.: The pre-reversal enhancement of the zonal electric field in the equatorial ionosphere, *J. Geophys. Res.*, 91, 13723–13728, 1986.
- Fejer, B. G., de Paula, E. R., Gonzales, S. A., and Woodman, R. F.: Average vertical and zonal plasma drift over Jicamarca, *J. Geophys. Res.*, 96, 13901–13906, 1991.
- Fejer, B. G., de Paula, E. R., Heelis, R. A., and Hanson, W. B.: Global equatorial ionosphere vertical plasma drifts measured by the AE-E satellite, *J. Geophys. Res.*, 100, 5769–5776, 1995.
- Gulyaeva, T. L.: Progress in ionospheric informatics based on electron density profile analysis of ionogram, *Adv. Space Res.*, 7, 39–48, 1987.
- Gulyaeva, T. L.: Variable coupling between the bottomside and top-side thickness of the ionosphere, *J. Atmos. Solar Terr. Phys.*, 69, 528–536, doi:10.1016/j.jastp.2006.10.015, 2007.
- Heelis, R. A.: Electrodynamics in the low and middle latitude ionosphere: a tutorial, *J. Atmos. Solar Terr. Phys.*, 66, 825–838, 2004.
- Krishnamurthy, B. K., Hari, S. S., Somayajulu, V. V.: Nighttime equatorial thermospheric meridional winds from ionospheric  $h'F$  data, *J. Geophys. Res.*, 95, 4307–4310, 1990.
- Lazo, B., Olazábal, K. A. C., Rodríguez González, M., and Calzadilla Méndez, A.: Diurnal variation of B parameters over Havana at low solar activity, *Geofísica Internacional*, 43, 125–128, 2004.
- Lazo, B., Savio, S., Alazo, K., Calzadilla, A., and Ojeda, A.: Diurnal variation of B parameters over Havana at low and high solar activity, *Adv. Space Res.*, 39, 711–714, 2007.
- Lee, C. C. and Reinisch, B. W.: Quiet-condition  $hmF2$ ,  $NmF2$ , and  $B0$  variations at Jicamarca and comparison with IRI-2001 during solar maximum, *J. Atmos. Sol.-Terr. Phys.*, 68, 2138–2146, 2006.
- Lee, C. C., Reinisch, B. W., Su, S.-Y., and Chen, W. S.: Quiet-time variations of F2 layer parameters at Jicamarca and comparison with IRI-2001 during solar minimum, *J. Atmos. Solar Terr. Phys.*, 70, 184–192, 2007.
- Lei, J., Liu, L., Wan, W., Zhang, S.-R., and Holt, J. M.: A statistical study of ionospheric profile parameters derived from Millstone Hill incoherent scatter radar measurements, *Geophys. Res. Lett.*, 31, L14804, doi:10.1029/2004GL020578, 2004.
- Liu, J. Y., Chuo, Y. J., Shan, S. J., Tsai, Y. B., Chen, Y. I., Pulinets, S. A., and Yu, S. B.: Pre-earthquake ionospheric anomalies registered by continuous GPS TEC measurements, *Ann. Geophys.*, 22, 1585–1593, doi:10.5194/angeo-22-1585-2004, 2004.
- Maruyama, T., Kawamura, M., Saito, S., Nozaki, K., Kato, H., Hemmakorn, N., Boonchuk, T., Komolmis, T., and Ha Duyen, C.: Low latitude ionosphere-thermosphere dynamics studies with inosonde chain in Southeast Asia, *Ann. Geophys.*, 25, 1569–1577, doi:10.5194/angeo-25-1569-2007, 2007.
- McKinnell, L.-A., Chimidza, O., and Cilliers, P.: The variability and predictability of the IRI B0, B1 parameters over Grahamstown, South Africa, *Adv. Space Res.*, 44, 747–755, 2009.
- Oladipo, O., Adeniyi, J., Radicella, S., and Adimula, I.: Variability of the ionospheric electron density at fixed heights and validation of IRI-2007 profile's prediction at Ilorin, *Adv. Space Res.*, 47, 496–505, 2011.
- Prölss, G. W.: Ionospheric F-region storms, in: *Handbook of Atmospheric Electrodynamics*, edited by: Volland, H., vol. 2, CRC Press, Boca Raton, FL, pp. 195–248, 1995.
- Ramakrishnan, S. and Rawer, K.: Model electron density profiles obtained by empirical procedures, in *Space Research XII, Proceedings of the Fourteen Plenary Meeting, Seattle, Wash; German Democratic Republic; 18 June–2 July 1971*, pp. 1253–1259, Akademie, Berlin, 1972.
- Rawer, K., Bilitza, D., and Ramakrishnan, S.: Goals and status of the International Reference Ionosphere, *Rev. Geophys.*, 16, 177–181, 1978.
- Reinisch, B. W. and Huang, X.: Low latitude digisonde measurements and comparison with IRI, *Adv. Space Res.*, 18, 5–12, 1996.
- Rishbeth, H., Fuller-Rowell, T. J., and Ress, D.: Diffusive equilibrium and vertical motion in the thermosphere during a severe magnetic storm: a computational study, *Planet. Space Sci.*, 35, 1157–1165, 1987.
- Rush, C., Fox, M., Bilitza, D., Davies, K., McNamara, L. F., Stewart, F., and Pokempner, M.: Ionospheric Mapping – An update of  $foF2$  coefficients, *Telecom J.*, 56, 179–182, 1989.
- Schunk, R. W. and Nagy, A. F.: *Ionospheres: Physics, Plasma Physics, and Chemistry*, in: Dessler, A. J., Houghton, J. T., and Rycroft, M. J., Cambridge Atmospheric and Space Science Series, Cambridge University Press, United Kingdom, 2000.
- Sethi, N. K. and Mahajan, K. K.: The bottomside parameters  $B0$ ,  $B1$  obtained from incoherent scatter measurements during a solar maximum and their comparisons with the IRI-2001 model, *Ann. Geophys.*, 20, 817–822, doi:10.5194/angeo-20-817-2002, 2002.
- Sethi, N., Dabas, R., and Upadhyaya, A.: Midday bottomside electron density profiles during moderate solar activity and comparison with IRI-2001, *Adv. Space Res.*, 43, 973–983, 2009.
- Stening, R. J.: Modeling the low-latitude F-region, A review, *J. Atmos. Solar Terr. Phys.*, 54, 1387–1412, 1992.
- Titheridge, J. E.: *Ionogram analysis with generalized program POLAN*, Rep. UAG-93, World Data Cent. A for Sol.-Terr. Phys., Boulder, Colorado, 1985.
- Zhang, M. L., Shi, J. K., Wang, X., Wu, S. Z., and Zhang, S. R.: Comparative study of ionospheric characteristic parameters obtained by DPS-4 digisonde with IRI 2000 for low latitude station in China, *Adv. Space Res.*, 33, 869–873, 2004.